Received: 15 April 2020 | Revised: 26 June 2020 | Accepted: 17 July 2020

DOI: 10.1002/app.49769

ARTICLE

Applied Polymer SCIENCE WILEY

Kinetics of the glass transition of styrene-butadiene-rubber: Dielectric spectroscopy and fast differential scanning calorimetry

Niclas Lindemann[1,2] | Jürgen. E. K. Schawe[3] | Jorge Lacayo-Pineda[2,4]

[1]Institut für Physikalische Chemie und Elektrochemie, Leibniz Universität Hannover, Hanover, Lower Saxony, Germany

[2]Department of Research and Development, Continental Reifen Deutschland GmbH, Hanover, Lower Saxony, Germany

[3]Mettler-Toledo GmbH, Nänikon, Zürich, Switzerland

[4]Institut für Anorganische Chemie, Leibniz Universität Hannover, Hanover, Lower Saxony, Germany

Correspondence
Niclas Lindemann, Leibniz Universitat Hannover, Institut für Physikalische Chemie und Elektrochemie, Callinstraße 3A, Hanover, Lower Saxony 30167, Germany.
Email: niclas.lindemann@pci.uni-hannover.de

Funding information
European Union's Horizon 2020 research and innovation program, Grant/Award Number: 760907; Open access funding enabled and organized by Projekt DEAL.

Abstract

The glass transition is relevant for performance definition in rubber products. For extrapolation to high-frequency behavior, time–temperature superposition is usually assumed, although most complex rubber compounds might be outside of its area of validity. Fast differential scanning calorimetry (FDSC) with cooling rates up to 1500 K/s and broadband dielectric spectroscopy (BDS) with frequencies up to 20 MHz are applied here to directly access both kinetics and dynamics of glass formation in a wide frequency range. For the first-time, the relation between the thermal vitrification and the dielectric relaxation is studied on vulcanized styrene-butadiene rubber, showing that both cooling rate and frequency dependence of its glass transition can be described by one single Vogel-Fulcher-Tammann-Hesse equation. The results indicate the validity of the Frenkel-Kobeko-Reiner equation. Another focus is the sample preparation of vulcanized elastomers for FDSC and BDS as well as the temperature calibration below 0°C.

KEYWORDS

dielectric properties, glass transition, kinetics, rubber, thermal properties

1 | INTRODUCTION

The analysis of the kinetics of the glass transition of elastomers is important for studying the influence of the molecular structure,[1,2] the network system,[3] and the polymer filler interaction[4,5] on the vitrification. Elastomeric-based materials are commonly used in the rubbery state. Thus, the kinetics just above the glass transition range is important for the properties of rubber. The glass transition is usually measured with conventional differential scanning calorimetry (DSC).

In rubber technology, the dynamics of the glass transition are widely studied by conventional dynamic mechanical analysis (DMA) typically up to frequencies of 100 Hz. An extrapolation to higher frequencies is performed by using the so-called time–temperature superposition principle (TTS).[6,7] The underlying assumption of TTS is the temperature invariance of the shape of the

mechanical relaxation spectrum. This means that the spectral distribution of the mechanical response is independent of the temperature and that only the mean relaxation time decreases with increasing temperature. This is a strong assumption, and although the master curve often appears smooth, there is no guarantee that the TTS principle is fulfilled. The risk of leaving the area of validity of TTS becomes evident when adding softeners, accelerators, fillers and other polymers into the elastomer compound. To avoid the use of TTS, other techniques, like broadband dielectric spectroscopy (BDS), are increasingly used to enlarge the frequency range on the high-frequency side.[8,9]

Calorimetric techniques enable the determination of the dynamic, frequency dependent, glass transition,[10–12] and the scanning rate-dependent vitrification and devitrification process[13] as well as the enthalpy relaxation in the glassy state.[14] The dynamic glass transition is a thermal relaxation process in a structural equilibrated supercooled melt characterized by the relaxation time, τ, and the dynamic glass transition temperature, $T_{g,\omega}$. The vitrification process is the transformation of the structural equilibrated supercooled highly viscose (rubbery) melt in a structural nonequilibrated glassy state with solid characteristics, which depends on the cooling rate, β_c.[15,16] In the past, several empirical relations between β_c and τ were discussed.[15–18] With the development of the fast differential scanning calorimetry (FDSC),[19,20] it is possible to study the vitrification process in a wide cooling rate range of more than six decades.[21,22] This enables a direct correlation between relaxation and vitrification.[23]

There are many reports of FDSC measurements of the cooling rate dependence of vitrification on polymers with a high-glass transition temperature (thermoplastics).[21,24–26] To the best of our knowledge, FDSC measurements on vulcanized rubbers have not been previously published. The reasons could be the relatively small dynamic range due to their low-glass transition temperature, and problems regarding sample preparation.

In this article, we study the kinetics of relaxation and vitrification in a wide range of frequency and cooling rate, respectively, on the example of a vulcanized, unfilled solution styrene-butadiene rubber compound (SBR). The relaxation measurements are performed by BDS. Vitrification is examined in a cooling rate range of ca. 6.5 decades with FDSC. Another focus of this work is on the specific requirements for sample preparation of elastomers and the improvement of the experimental conditions for the FDSC, such as the thermal contact between sample and sensor as well as the accuracy of temperature measurement.

TABLE 1 Compound formulation

Substance	SBR compound (phr[a])	SBR compound (wt%)
SBR[b]	100	87.7
6PPD[c]	2.0	1.8
Wax	2.0	1.8
Zinc oxide	2.5	2.2
Stearic acid	2.5	2.2
Vulcanization system		
DPG[d]	1.0	0.9
CBS[e]	2.0	1.8
Sulfur	2.0	1.8

Abbreviation: SBR, styrene-butadiene rubber.
[a]Parts per hundred rubber, non-SI unit, for example, mass of a component in g per 100 g of raw rubber.
[b]Microstructure: 24.3% styrene, 33.0% vinyl, 27.7% cis, 39.3% *trans*.
[c]N-(1,3-Dimethylbutyl)-N′-phenyl-p-phenylenediamine.
[d]1,3-Diphenylguanidine.
[e]N-Cyclohexylbenzothiazol-2-sulfenamide.

2 | EXPERIMENTAL

2.1 | Materials

2.1.1 | Elastomer

The material of investigation is an unfilled vulcanized solution SBR according to the formulation in Table 1.

The compound was mixed in a two-step mixing process with a 2 liters internal mixer (Harburg-Freudenberger, Germany) using a tangential two-wing rotor. In the first step, all ingredients except the vulcanization system were mixed for 7:20 min. The ejection temperature was 155°C. After adding the vulcanization system in the second step, the compound was mixed for 3.5 min at 110°C. Samples were vulcanized at 160°C for 18 min to reach 95% cross-linking.

2.1.2 | Calibration material

For calibration purposes of all instruments, adamantane (purity ≥99%) from Acros Organics, Belgium, was used. Adamantane has been recommended for low temperature calibration of conventional DSC.[27,28] The fcc to bcc solid–solid transition occurs at -64.43 ± 0.05°C with a high repeatability and precision.[29,30] This material is selected because the transformation temperature is in the range of the glass transition of many elastomers, and the sublimation pressure during preparation at ambient

conditions is much lower compared to the vapor pressure of other potential calibration substances like cyclopentane or n-octane.[29,31]

2.2 | Broadband dielectric spectroscopy

The dielectric measurements were performed with an Alpha-A High-Performance Frequency Analyzer with a Novocool cryo-system (Novocontrol Technologies, Germany). The accuracy of the cryostat is ±0.3 K. Frequency sweeps between 0.1 and $2{\cdot}10^6$ Hz were performed in the temperature range of −100 to 100°C in five-degree steps. The measurement was performed in a plate capacitor arrangement with a capacitance of $C^*(\omega) = \varepsilon^*(\omega)\pi D^2/4d$, where ω is the angular frequency, ε^* the complex permittivity, D the diameter and d the thickness. The permittivity $\varepsilon^*(\omega) = C^*(\omega)/C_0$ was determined using the capacitance of the empty measurement cell, C_0.

The sample temperature in the measurement cell was verified by measuring an adamantane plate with a thickness of 150 µm at a heating rate of 0.1 K/min in a temperature interval between −85 and −45°C. The measuring frequency was 100 Hz. Figure 1(a) displays the peak of the first derivative of the permittivity due to the phase transition of adamantane. The onset temperature was used for calibration. Hence, a temperature correction of +0.4 K is needed.

2.3 | Conventional differential scanning calorimetry

Conventional DSC measurements were conducted with a DSC1 (Mettler-Toledo, Switzerland) equipped with the liquid nitrogen cooling option and the HSS-8 sensor. Hermetically sealed, standard Al-crucibles with a volume of 40 µl were used for all measurements. The DSC was previously adjusted with water, indium and zinc. A heating measurement of 1.5 mg adamantane with 10 K/min verifies the adjustment at low temperatures. The DSC curve is plotted in Figure 1(b). The onset is 0.2 K below the literature value; and therefore, the measured temperatures were corrected accordingly.

For preparation of the SBR sample, a cylinder (diameter: 4 mm) was drilled out of a vulcanized rubber block with an Alztronic 16 drilling machine (Alzmetall, Germany). The final sample is a sheet of about 0.8 mm thickness cut with a sharp razor blade, and a weight of about 10 mg. The measurements were performed between −110 and 40°C at the scanning rate of 10 K/min. It was cooled and subsequently heated. In between these scanning segments, the instrument was equilibrated for 20 min.

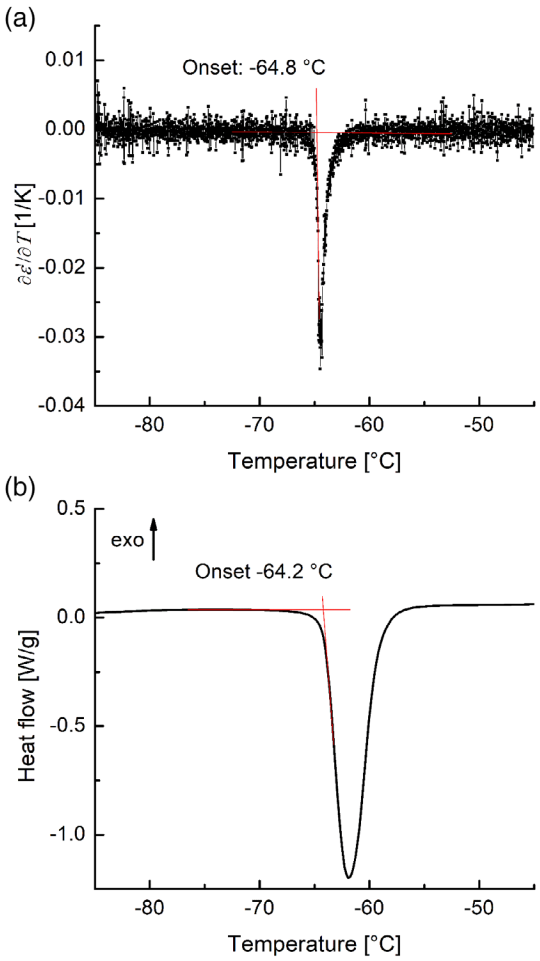

FIGURE 1 (a) Peak of the first derivative of the real part of the permittivity due to the phase transition of adamantane measured by BDS (heating rate 0.1 K/min). (b) Phase transition peak of adamantane obtained by DSC (heating rate 10 K/min). BDS, broadband dielectric spectroscopy; DSC, differential scanning calorimetry [Color figure can be viewed at wileyonlinelibrary.com]

2.4 | Fast differential scanning calorimetry

The FDSC experiments were performed using a Flash DSC 1 (Mettler-Toledo, Switzerland) equipped with an Intracooler TC100 (Huber, Germany) to reach the low temperature needed for analysis of the glass transition in elastomers. Nitrogen gas with a flow rate of 20 ml/min was purged through the UFS1 sensor. The sensor support temperature during the measurement was set to −95°C.

The FDSC technique with removable sensors was developed for calorimetry at fast heating and cooling rates up to several thousand Kelvin per second to study fast kinetic processes. In order to fulfill these conditions, a small DSC furnace and a small sample mass are required to reach an acceptable thermal lag. The furnace is built on a thin silicon nitrate membrane with the active

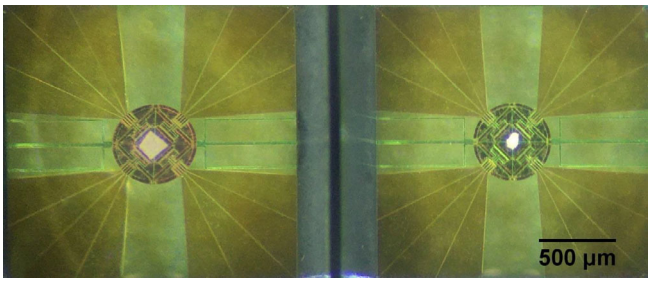

FIGURE 2 Furnaces of the UFS1 sensor with samples. The circular structures are the furnace areas. The structures inside and outside the furnaces arise from electrical components. Samples are placed in the center of the furnace. Left: SBR (sample side), right: Adamantane (reference side). SBR, styrene-butadiene rubber compound [Color figure can be viewed at wileyonlinelibrary.com]

furnace area in the center, where the small sample is placed as shown in Figure 2. On the left side in Figure 2, SBR has been placed on the sample area. Adamantane has been placed on the reference area for a post-measurement calibration (right side of Figure 2).

Because of the small sample mass—in contrast to conventional DSC—the sample has nearly the same heat capacity as the furnace. To improve the thermal contact, the sensor is not encapsulated. For fast cooling rates, cooled gas is required. A sufficiently thin sample is essential to keep the static and dynamic temperature gradients small. For further details on this measurement technique, see Reference 32.

As mentioned above, high quality FDSC results require thin samples with a good thermal contact to the removable sensor. The typical sample thickness for polymers is ≤10 µm.[21,33,34] Due to the comparable heat conduction,[35,36] this limit is also valid for rubber. However, vulcanized rubber cannot be melted to ensure the thermal contact, like thermoplastics. The alternative of using a contact medium such as silicon oil is inappropriate at low temperatures. Hence, to guarantee the quality of the thermal contact for rubber samples, a more careful preparation is required to create an absolutely flat, stress-free, and flexible sample.

For this purpose, the vulcanized rubber samples were pre-cut to an elongated cuboid of about 1 mm^2 cross-section. This cuboid was cut into sections with the thickness of 6 µm using a cryo-microtome MT-990 (RMC Boeckeler) equipped with a glass knife at −60°C with a cutting speed of 1 mm/s. The thin slices were cut with a scalpel to attain the final sample shape with an area of about 150 µm^2, which is comparable to the center of the active zone of the sensor. The thin slice was carefully placed with a so called eyelash manipulator (very soft and fine hair tip) within the active zone to ensure a good thermal contact[37] (Figure 2).

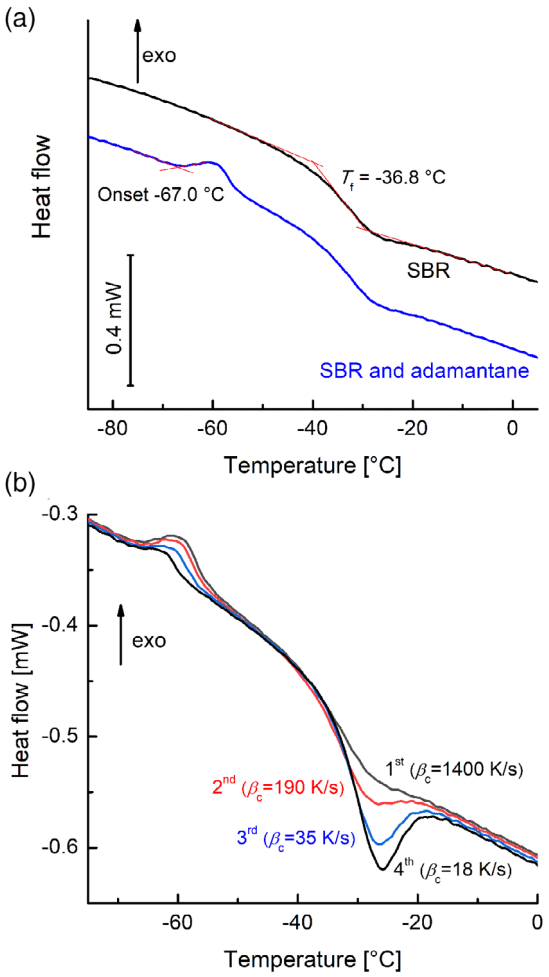

FIGURE 3 FDSC curves measured at heating rates of 1000 K/s. (a) Measurement curves for SBR with and without adamantane after cooling at 1000 K/s. (b) Measured curves of SBR with adamantane on the reference side after cooling at different rates. The adamantane peak and the enthalpy relaxation of SBR appear at ca. −60°C and ca. −25°C, respectively. FDSC, fast differential scanning calorimetry; SBR, styrene-butadiene rubber compound [Color figure can be viewed at wileyonlinelibrary.com]

In Figure 3(a), the difference between the measured onset (−67.0°C) and the temperature of the solid–solid transition of adamantane (−64.4°C) is +2.6 K. All samples measured with the same experimental setup (chip-sensor, gas type, flow rate, etc.) must be corrected by this value. This uncertainty is typical for the specific setup. Thus, a post-measurement calibration is required. For this purpose, the adamantane was placed on the reference side of the sensor after performing the sample measurements (Figure 3(a)). Note that in Figure 3(a), the peak of the adamantane transition appears in the exotherm direction, because the calibration sample is located on the reference side of the calorimeter.

Shoifet et al. propose to use "special precautions" for the calibration of chip calorimeters with adamantane due

to its fast sublimation.[38] Figure 3(b) clearly shows the decrease of the peak intensity of adamantane with increasing measurement time due to sublimation. This figure shows a selection of heating curves after increasing the total measuring time. The decreased peak intensity of the adamantane transformation has no influence on the peak onset.

3 | RESULTS AND DISCUSSION

The spectra of the dielectric loss component of the permittivity, ε'', of SBR at different temperatures are shown in Figure 4(a). The main peak represents the α-relaxation. At low frequencies, the conductivity contribution, $\sigma(\omega)$, dominates the measured curves. It is $\sigma(\omega) = -i\,\sigma_0/(\varepsilon_0\omega)$, where σ_0 is the specific DC conductivity and ε_0 is the vacuum permittivity.

The α-relaxation is a dipole relaxation due to the cooperative rearrangements of polymer chain segments. This process is also referred to the dielectric glass transition. Inhomogeneities in the local surrounding of the polymer chain segments (intramolecular interactions, e.g. microstructure[39]) lead to a broadening on the high-frequency side. Large scale correlations (intermolecular interactions, e.g. cross-linking[8]) broaden the low-frequency side of the α-relaxation.[40] Commonly, the relaxation process is modeled by the Havriliak-Negami function:

$$\varepsilon^*(\omega) = \varepsilon'(\omega) - i\varepsilon''(\omega) = \varepsilon_\infty + \frac{\Delta\varepsilon}{(1+(i\omega\tau)^\alpha)^\beta}, \qquad (1)$$

where i is the imaginary unit, ε_∞ is the high-frequency limit of the real part of the permittivity, $\Delta\varepsilon$ is the relaxation strength, τ is the characteristic relaxation time and α, β are the shape parameters of the relaxation process. The parameter α characterizes the slope of the log ε'' versus log ω peak on the low-frequency side, while the product $\alpha\beta$ on the high-frequency side of the relaxation, respectively.

In contrast to most polymers, the α-relaxation process of SBR is symmetric.[8,41,42] Thus, the relaxation can be described with $\beta = 1$, this is the so-called Cole-Cole function:

$$\varepsilon^*(\omega) = \varepsilon_\infty + \frac{\Delta\varepsilon}{1+(i\omega\tau)^\alpha}. \qquad (2)$$

The characteristic relaxation time τ is determined from the peak maximum of the ε'' peak by $\omega_{max}\,\tau \approx 1$, where ω_{max} is the angular frequency at the maximum of the fitted relaxation function.

Figure 4(a) shows an asymmetric relaxation peak due to a shoulder on the low-frequency side. This asymmetric relaxation peak clearly contains at least two contributions with different temperature dependencies as the peak broaden with decreasing temperature. Ortega et al. assign the low-frequency broadening of the loss peak as additional mode, and recommend the separation of the two processes applying two Cole-Cole functions.[42]

Hence, the complete measured curves in Figure 4(a) can be described by:

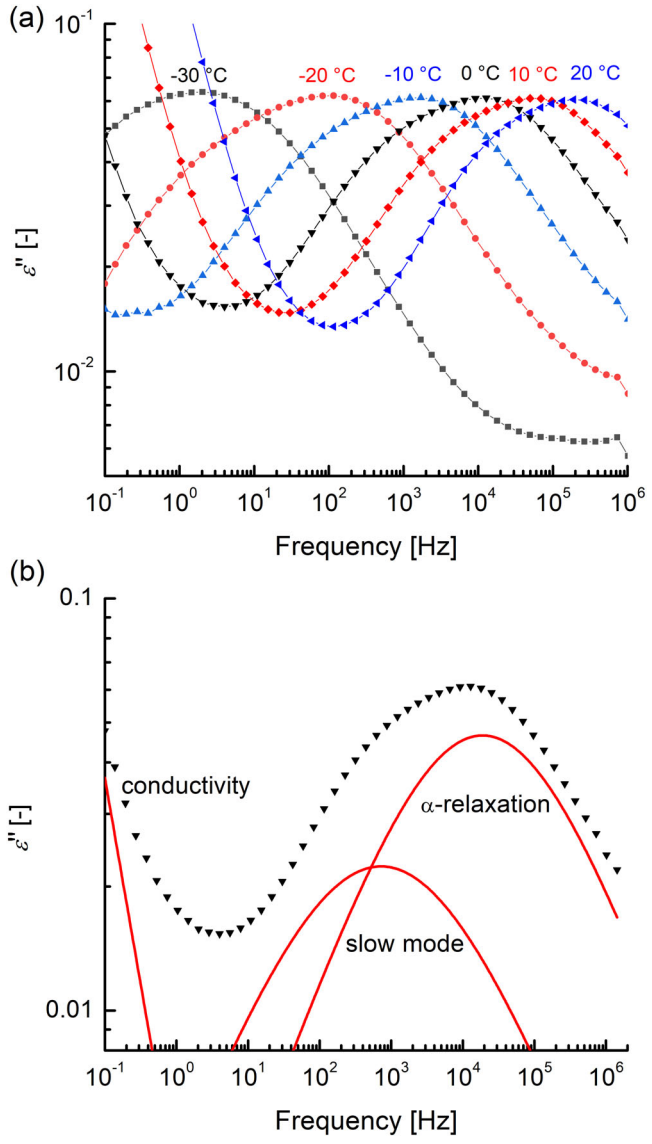

FIGURE 4 Dielectric losses (ε'') as function of the frequency of SBR. (a) Curves at different temperatures. Solid lines are just guides for the eyes. (b) Curve at 0°C including the fit functions of the three contributions. SBR, styrene-butadiene rubber compound [Color figure can be viewed at wileyonlinelibrary.com]

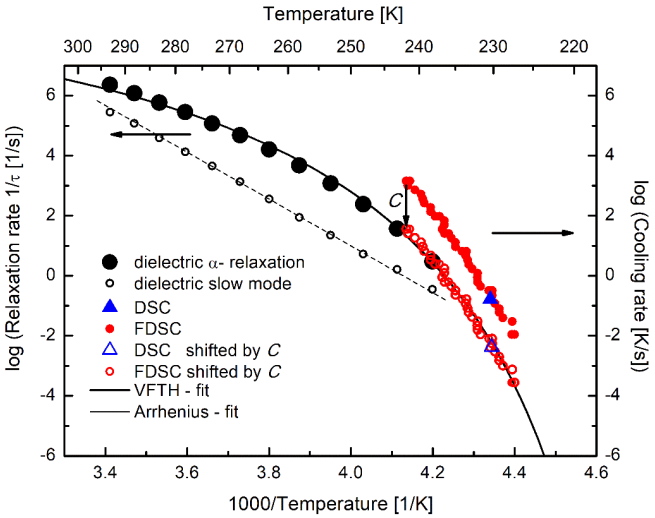

FIGURE 5 Activation diagram of SBR. The left ordinate is the logarithm of the reciprocal dielectric relaxation time. The right ordinate is the logarithm of the cooling rate of both DSC and FDSC. The abscissa characterizes the measurement temperature of the dielectric measurements and the fictive temperature determined from the DSC and FDSC measurements, respectively. After shifting the cooling rate by the factor C, DSC and FDSC data can be fitted together with the dielectric α-relaxation with the VFTH equation. DSC, differential scanning calorimetry; FDSC, fast differential scanning calorimetry; SBR, styrene-butadiene rubber compound; VFTH, Vogel-Fulcher-Tammann-Hesse [Color figure can be viewed at wileyonlinelibrary.com]

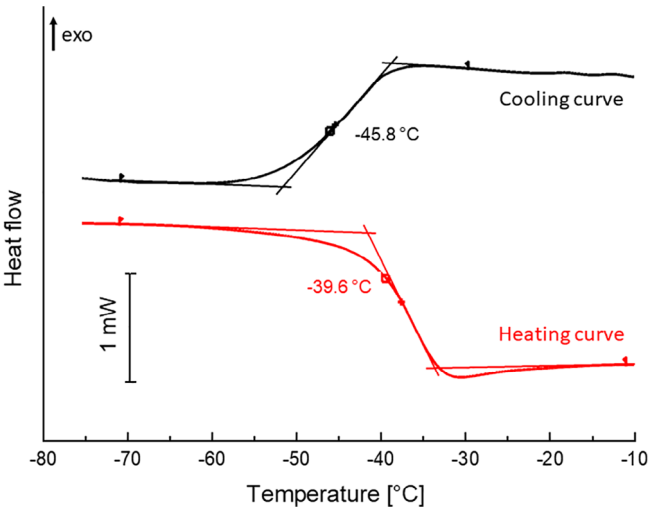

FIGURE 6 DSC curves of the glass transition region measured during cooling and subsequent heating at ±10 K/min. The evaluation of the limiting fictive temperatures is shown. The reported temperatures still require a correction by +0.2 K (adamantane calibration). DSC, differential scanning calorimetry [Color figure can be viewed at wileyonlinelibrary.com]

$$\varepsilon^*(\omega) = \varepsilon_\infty + \sum_{k=1}^{2} \frac{\Delta\varepsilon_k}{1+(i\omega\tau_k)^{\alpha_k}} - i\sigma_0/(\varepsilon_0\omega). \quad (3)$$

This function is used for separation of the different contributions by curve fitting as shown in Figure 4(b).

Figure 5 shows the temperature dependence of the relaxation rates, $1/\tau$, of the α-relaxation (filled black circles). This temperature dependence corresponds to the Vogel-Fulcher-Tammann-Hesse (VFTH) equation,[43–46] as expected for glass forming polymer systems:

$$\log(1/\tau) = A - \frac{B}{T - T_V}, \quad (4)$$

where A is the logarithm of the pre-exponent factor, B the curvature parameter related to the fragility[47] and T_V the Vogel temperature.

In agreement with Reference 48, the slow mode (open black circles in Figure 5) follows the Arrhenius equation

$$\log(1/\tau) = A_A - \frac{E_a \ln 10}{RT}, \quad (5)$$

where A_A is the logarithm of the pre-exponent factor, E_a the apparent activation energy and R the gas constant. These parameters are determined by least square fit to be $A_A = 32.2$ and $E_a = 149$ J/mol.

The pre-exponential factor indicates that the slow mode might change its behavior at higher temperatures, suggesting that it might unify with the α-relaxation process. The high-activation energy of this process is not comparable to the one of the secondary β-relaxation of approximately 34 J/mol.[39] The slow mode process occurs due to the presence of the vulcanization accelerator 1,3-Diphenylguanidine (DPG). It can be assumed that the dipoles of the DPG couple to the SBR chain segments instead of having an independent relaxation process.[42]

The cooling rate dependence of the vitrification process measured by DSC is characterized by the limiting fictive temperature, T_f, related to the structure of the glassy state after cooling.[49] At temperatures below the vitrification process, the glass has the same configurational entropy at the sample temperature, T, as a supercooled structurally equilibrated melt at $T_f > T$. From the heat flow curve, $\Phi(T)$, T_f is determined by considering the extrapolation of the liquid state, $\Phi_l(T)$, and the glassy state, $\Phi_g(T)$, according to References 49 and 50:

$$T_f = T_{rl} - \int_{T_{rg}}^{T_{rl}} \frac{\Phi(T) - \Phi_g(T)}{\Phi_l(T) - \Phi_g(T)} dT, \quad (6)$$

where T_{rl} and T_{rg} are reference temperatures in the supercooled liquid and the glassy state, respectively. Theses temperatures are outside the glass transition range. Here, the glass transition temperature is defined as the limiting fictive temperature.

Conventional heat flow curves of the glass transition of SBR measured both during cooling and subsequent heating at scanning rates of ±10 K/min are shown in Figure 6. According to the energy conservation law, the limiting fictive temperature of the cooling and the subsequent heating measurement are identical.[51] Deviations are the consequence of the thermal lag, which can be corrected by averaging both limiting fictive temperatures.[21,52] From the measurements shown in Figure 6, the limiting fictive transition temperature is determined to be $T_f = -42.5°C$ considering the post-measurement calibration with adamantane.

The cooling rate dependence of the glass transition can be measured by FDSC in a range of more than six decades. There are two different methods to measure the cooling rate dependence of T_f:

- The first method is to measure the cooling and subsequent heating curves with the same absolute scanning rate (cooling rate = −heating rate).[21] As mentioned above, T_f is the average of the two measured temperatures. The advantage of this method is that large enthalpy relaxation peaks are avoided. The disadvantage is the relatively narrow scanning rate range. The decreased sensitivity at low-cooling rates precludes the correct determination of the fictive temperature.

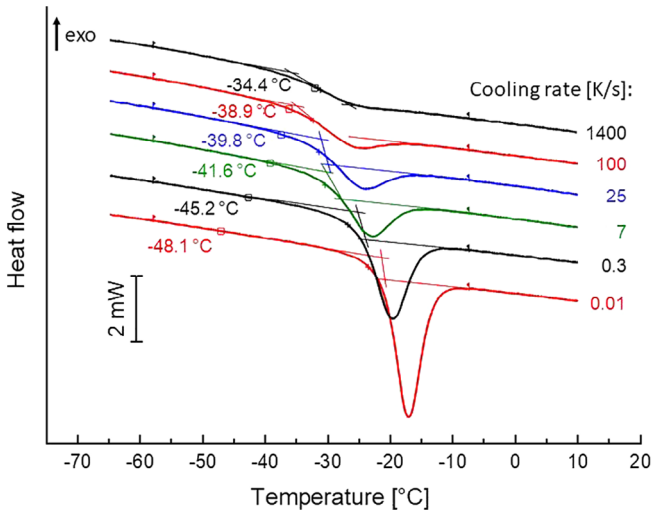

FIGURE 7 Collection of FDSC heating curves at 1000 K/s with indicated T_f measured after different cooling rates. Temperature evaluation still requires a correction by +2.6 K (adamantane calibration). FDSC, fast differential scanning calorimetry [Color figure can be viewed at wileyonlinelibrary.com]

- The other method frequently used is to cool the sample at various rates and subsequently heat it with the same rate every time.[22,53,54] The heating rate is selected in such a way that the measurement has a good sensitivity and the influence of the thermal lag is low. This method has the advantage that the limiting fictive temperature can be determined also for very slow cooling rates. The disadvantage is, however, that relatively large overheating peaks occur after slow cooling. This complicates the evaluation of T_f.

To reach the maximum range of the cooling rate for this investigation, the second method was applied with a heating rate of 1000 K/s. For this conditions, the thermal lag can be widely disregarded.[21] This was confirmed by applying the first method in a limited scanning rate interval (100–1000 K/s). Figure 7 displays several selected heating curves measured after different cooling rates indicating their respective limiting fictive temperature. As expected, increasing the cooling rate increases T_f.

Based on polystyrene as an example, it has been shown that the relation between the relaxation frequency and the cooling rate follows the Frenkel-Kobeko-Reiner (FKR) equation in a good approximation[23]:

$$\log(\beta_c \tau / 1\mathrm{K}) = C, \tag{7}$$

where β_c is the cooling rate and C is the shift parameter. The corresponding relaxation time of the glass transition measured in the conventional DSC at 10 K/min is frequently approximated to a value between 100 and 1000 s.[16,18,55–57] Thus, C is expected to be in between 1.2 and 2.2.

Several investigations[12,24,58–61] show that the relaxation times of the dielectric permeability and the heat capacity are almost identical. Therefore, the dielectric and thermal results can be combined by shifting the DSC and FDSC data by C. This procedure is visualized in Figure 5. The shift parameter $C = 1.6$ can be found by the best overlap of the different data sets. This result is in a good agreement with the finding for polystyrene ($C = 1.5$).[23]

After shifting the calorimetric data, the combined activation curve is fitted with the VFTH equation (Figure 5). The fit parameters are $A = 9.95$, $B = 343$ K, and $T_v = 202$ K.

According to References 23, 62, and 63 the dynamic fragility, m, can be determined from the VFTH parameters by

$$m = \frac{BT}{(T - T_V)^2}. \tag{8}$$

If T is the glass transition temperature measured with conventional DSC at 10 K/min (230.6 K), the fragility is

$m = 96.7$. The fragility depends on the molecular composition of the copolymers. In consideration of this fact, $m = 96.7$ corresponds to reported data of different non-vulcanized SBR types between 69 and 84.[39] An additional effect on the fragility could be caused by the influence of cross-linking on the glass transition of SBR.

By combination of FDSC, BDS, and the application of the FKR equation, the time–temperature relation of the glass transition of SBR is determined in a range of relaxation time of more than 10 decades. The shift factor between the cooling rate and the relaxation time is determined by the best overlap between dielectric and calorimetric data. To our knowledge, this is the first successful application of the FKR equation for a vulcanized rubber material.

4 | CONCLUSIONS

The temperature time dependence of relaxation processes is essential for the prediction of material properties like rolling resistance and traction of tires. This discussion is commonly based on the so-called TTS.[6,7] The complexity of modern elastomer compounds requires the direct measurement of relaxation behavior.[64] Independent techniques, such as FDSC and BDS, are required to directly access both the kinetics of the thermal vitrification and the dynamic of the glass forming process at high frequencies.

For both techniques, BDS and FDSC, specific requirements for sample preparation need to be considered when investigating elastomers since them, unlike thermoplastics, cannot be melted into a shape. In order to reach the capacitance required for accurate BDS measurements, samples are molded in a curing press to a thickness of about 100–200 µm. In order to avoid thermal lags in FDSC, cryomicrotomic slices of 6 µm have proven to be appropriate.

The temperature correction for FDSC was implemented using the solid–solid transition of adamantane at −64.4°C. For the specific FDSC setup in this work (including purged gas and flow, sensor, etc.), the temperature correction was 2.6 K. The seemingly high value is reasonable due to the high-cooling rate of up to 1500 K/s.

In addition to the temperature correction, the thermal glass transition temperatures were shifted according to the FKR Equation (7). With this approach, the cooling rate and frequency dependence of the glass transition of SBR can be described by one single VFTH-Equation (4). While the FKR equation has been already validated for thermoplastics,[21,59] vulcanized styrene-butadiene rubber has been studied here for the first-time. The value obtained for the shift parameter $C = 1.6$ confirms the expectations. The experimental approach of a carefully performed temperature calibration enables the use of the FDSC technique in combination with BDS in elastomer research. Future investigations will involve a systematic study of filled elastomers so as to give a more general statement on the current findings.

ACKNOWLEDGMENTS

The authors gratefully acknowledge helpful discussions with D. Wilmer (Novocontrol Technologies), F. Kremer (Universität Leipzig) and A. Karimi (Continental Tires) as well as the permission for publication granted by Continental Tires. This project has received funding from the European Union's Horizon 2020 research and innovation program under grant agreement No 760907. Open access funding enabled and organized by Projekt DEAL.

ORCID

Niclas Lindemann https://orcid.org/0000-0002-5247-0093

Jürgen. E. K. Schawe https://orcid.org/0000-0002-2246-2236

REFERENCES

[1] B. Stühn, *J. Polym. Sci., Part B: Polym. Phys.* **1992**, *30*, 1013.
[2] W. Stark, M. Jaunich, *Polym. Test.* **2011**, *30*, 236.
[3] H. Stutz, K.-H. Illers, J. Mertes, *J. Polym. Sci., Part B: Polym. Phys.* **1990**, *28*, 1483.
[4] H. Lu, S. Nutt, *Macromolecules* **2003**, *36*, 4010.
[5] D. Fragiadakis, P. Pissis, L. Bokobza, *Polymer* **2005**, *46*, 6001.
[6] J. D. Ferry, *Viscoelastic properties of polymers*, John Wiley & Sons, New York, Chichester, Brisbane, Toronto, Singapore **1980**.
[7] M. Klüppel, *J. Phys.: Condens. Matter* **2008**, *21*, 35104.
[8] A. Schönhals, in *Broadband dielectric spectroscopy* (Eds: F. Kremer, A. Schönhals), Springer, Berlin, Heidelberg **2003**. https://doi.org/10.1007/978-3-642-56120-7_7.
[9] J. Mijović, H. K. Lee, J. Kenny, J. Mays, *Macromolecules* **2006**, *39*, 2172.
[10] A. Boller, C. Schick, B. Wunderlich, *Thermochim. Acta* **1995**, *266*, 97.
[11] J. E. K. Schawe, *Thermochim. Acta* **1995**, *261*, 183.
[12] A. Hensel, J. Dobbertin, J. E. K. Schawe, A. Boller, C. Schick, *J. Therm. Anal.* **1996**, *46*, 935.
[13] C. T. Moynihan, A. J. Easteal, J. Wilder, J. Tucker, *J. Phys. Chem.* **1974**, *78*, 2673.
[14] I. M. Hodge, *J. Non-Cryst. Solids* **1994**, *169*, 211.
[15] E. Donth, *The glass transition: relaxation dynamics in liquids and disordered materials*, Springer, Berlin, Heidelberg **2001**.
[16] I. S. Gutzow, J. W. P. Schmelzer, *The vitreous state: thermodynamics, structure, rheology, and crystallization*, Springer, Dordrecht, The Netherlands **2013**.
[17] W. Heinrich, B. Stoll, *Prog. Colloid Polym. Sci.* **1988**, *78*, 37.
[18] G. W. Scherer, *J. Am. Ceram. Soc.* **1984**, *67*, 504.

[19] E. Zhuravlev, C. Schick, *Thermochim. Acta* **2010**, *505*, 1.
[20] V. Mathot, M. Pyda, T. Pijpers, G. Vanden Poel, E. van de Kerkhof, S. van Herwaarden, F. van Herwaarden, A. Leenaers, *Thermochim. Acta* **2011**, *522*, 36.
[21] J. E. K. Schawe, *Thermochim. Acta* **2015**, *603*, 128.
[22] J. E. K. Schawe, K.-U. Hess, *Thermochim. Acta* **2019**, *677*, 85.
[23] J. E. K. Schawe, *J. Chem. Phys.* **2014**, *141*, 184905.
[24] Y. Z. Chua, G. Schulz, E. Shoifet, H. Huth, R. Zorn, J. W. P. Schmelzer, C. Schick, *Colloid Polym. Sci.* **2014**, *292*, 1893.
[25] X. Monnier, D. Cangialosi, *Thermochim. Acta* **2019**, *677*, 60.
[26] N. Shamim, Y. P. Koh, S. L. Simon, G. B. McKenna, *J. Polym. Sci., Part B: Polym. Phys.* **2014**, *52*, 1462.
[27] G. Hakvoort, *J. Therm. Anal.* **1994**, *41*, 1551.
[28] G. Hakvoort, C. M. Hol, *J. Therm. Anal. Calorim.* **1999**, *56*, 717.
[29] A. B. Bazyleva, A. V. Blokhin, G. J. Kabo, M. B. Charapennikau, V. N. Emel'yanenko, S. P. Verevkin, V. Diky, *J. Phys. Chem. B* **2011**, *115*, 10064.
[30] S.-S. Chang, E. F. Westrum, *J. Phys. Chem.* **1960**, *64*, 1547.
[31] G. Hakvoort, C. M. Hol, P. J. van Ekeren, *J. Therm. Anal. Calorim.* **2002**, *69*, 333.
[32] J. E. K. Schawe, S. Pogatscher, in *Fast scanning calorimetry* (Eds: C. Schick, V. Mathot), Springer International Publishing, Switzerland **2016**, p. 3. https://doi.org/10.1007/978-3-319-31329-0_1.
[33] A. Toda, M. Konishi, *Thermochim. Acta* **2014**, *589*, 262.
[34] A. Toda, K. Taguchi, K. Nozaki, M. Konishi, *Polymer* **2014**, *55*, 3186.
[35] T. Bhowmick, S. Pattanayak, *Cryogenics* **1990**, *30*, 116.
[36] B. D. Washo, D. Hansen, *J. Appl. Phys.* **1969**, *40*, 2423.
[37] G. V. Poel, D. Istrate, A. Magon, V. Mathot, *J. Therm. Anal. Calorim.* **2012**, *110*, 1533.
[38] E. Shoifet, G. Schulz, C. Schick, *Thermochim. Acta* **2015**, *603*, 227.
[39] S. Cerveny, R. Bergman, G. A. Schwartz, P. Jacobsson, *Macromolecules* **2002**, *35*, 4337.
[40] A. Schönhals, E. Schlosser, *Colloid Polym. Sci.* **1989**, *267*, 125.
[41] G. A. Schwartz, L. Ortega, M. Meyer, N. A. Isitman, C. Sill, S. Westermann, S. Cerveny, *Macromolecules* **2018**, *51*, 1741.
[42] L. Ortega, S. Cerveny, C. Sill, N. A. Isitman, A. L. Rodriguez-Garraza, M. Meyer, S. Westermann, G. A. Schwartz, *Polymer* **2019**, *172*, 205.
[43] G. S. Fulcher, *J. Am. Ceram. Soc.* **1925**, *8*, 339.
[44] G. Tammann, W. Hesse, *Z. Anorg. Allg. Chem.* **1926**, *156*, 245.
[45] H. Vogel, *Phys. Z.* **1921**, *22*, 645.
[46] J. M. Alberdi, A. Alegríaa, E. Macho, J. Colmenero, *J. Polym. Sci., Part C: Polym. Lett.* **1986**, *24*, 399.
[47] Q. Qin, G. B. McKenna, *J. Non-Cryst. Solids* **2006**, *352*, 2977.
[48] Ortega Alvarez, L. Chain dynamics in crosslinked filled and unfilled polymer blends of different miscibility, Ph.D. Thesis, Donostia–San Sebastián, **2018**.
[49] C. T. Moynihan, A. J. Easteal, M. A. De Bolt, J. Tucker, *J. Am. Ceram. Soc.* **1976**, *59*, 12.
[50] M. J. Richardson, N. G. Savill, *Polymer* **1975**, *16*, 753.
[51] J. E. K. Schawe, *Thermochim. Acta* **2007**, *461*, 145.
[52] J. E. K. Schawe, *J. Polym. Sci., Part B: Polym. Phys.* **1998**, *36*, 2165.
[53] S. Gao, S. L. Simon, *Thermochim. Acta* **2015**, *603*, 123.
[54] N. G. Perez-de-Eulate, V. Di Lisio, D. Cangialosi, *ACS Macro Lett.* **2017**, *6*, 859.
[55] A. Cavagna, *Phys. Rep.* **2009**, *476*, 51.
[56] P. J. Carroll, G. D. Patterson, S. A. Cullerton, *J. Polym. Sci., Polym. Phys. Ed.* **1983**, *21*, 1889.
[57] K. Trachenko, C. M. Roland, R. Casalini, *J. Phys. Chem. B* **2008**, *112*, 5111.
[58] K. Schneider, E. Donth, *Acta Polym.* **1986**, *37*, 333.
[59] A. Dhotel, B. Rijal, L. Delbreilh, E. Dargent, A. Saiter, *J. Therm. Anal. Calorim.* **2015**, *121*, 453.
[60] B. Robles-Hernández, X. Monnier, J. A. Pomposo, M. Gonzalez-Burgos, D. Cangialosi, A. Alegría, *Macromolecules* **2019**, *52*, 6868.
[61] H. Huth, M. Beiner, E. Donth, *Phys. Rev. B* **2000**, *61*, 15092.
[62] R. Böhmer, C. A. Angell, *Phys. Rev. B: Condens. Matter* **1992**, *45*, 10091.
[63] F. Spieckermann, I. Steffny, X. Bian, S. Ketov, M. Stoica, J. Eckert, *Heliyon* **2019**, *5*, e01334.
[64] S. Napolitano, E. Glynos, N. B. Tito, *Rep. Prog. Phys.* **2017**, *80*, 36602.

How to cite this article: Lindemann N, Schawe JEK, Lacayo-Pineda J. Kinetics of the glass transition of styrene-butadiene-rubber: Dielectric spectroscopy and fast differential scanning calorimetry. *J Appl Polym Sci*. 2021;138:e49769. https://doi.org/10.1002/app.49769